

Article

Threat of Pollution Hotspots Reworking in River Systems: Case Study of the Ploučnice River (Czech Republic)

Jitka Elznicová * , Tomáš Matys Grygar, Jan Popelka , Martin Sikora, Petr Novák and Michal Hošek

Faculty of Environment, J.E. Purkyně University in Ústí nad Labem, Králova výšina 7, 40096 Ústí nad Labem, Czech Republic; grygar@iic.cas.cz (T.M.G.); jan.popelka@ujep.cz (J.P.); sikoramartin26@gmail.com (M.S.); petr.novak@ujep.cz (P.N.); psitlapa@seznam.cz (M.H.)

* Correspondence: jitka.elznicova@ujep.cz; Tel.: +420-475-284-136

Received: 14 December 2018; Accepted: 13 January 2019; Published: 16 January 2019



Abstract: As fluvial pollution may endanger the quality of water and solids transported by rivers, mapping and evaluation of historically polluted fluvial sediments is an urgent topic. The Ploučnice River and its floodplain were polluted by local uranium mining from 1971–1989. We have studied this river since 2013 using a combination of diverse methods, including geoinformatics, to identify pollution hotspots in floodplains and to evaluate the potential for future reworking. Archival information on pollution history and past flooding was collected to understand floodplain dynamics and pollution heterogeneity. Subsequently, a digital terrain model based on laser scanning data and data analysis were used to identify the sites with river channel shifts. Finally, non-invasive geochemical mapping was employed, using portable X-ray fluorescence and gamma spectrometers. The resulting datasets were processed with geostatistical tools. One of the main outputs of the study was a detailed map of pollution distribution in the floodplain. The results showed a relationship between polluted sediment deposition, past channel shifts and floodplain development. We found that increased concentration of pollution occurred mainly in the cut-off meanders and lateral channel deposits from the mining period, the latter in danger of reworking (reconnecting to the river) in the coming decades.

Keywords: geomorphic analysis; portable analytical instruments; geostatistical interpolation; pollution distribution

1. Introduction

Rivers and their floodplains store historical pollution, and river channels rework and return this contamination to fluvial transport. Notably, the first studies devoted to the risks of reworking of historically polluted fluvial sediments appeared in the geomorphology field [1–3]. Polluted floodplains in the Czech Republic also represent an environmental risk due to sediment reworking [4,5].

Geographic information systems (GIS) offer valuable tools for studying spatiotemporal changes in river channels and providing suitable fundamentals for fluvial geomorphologic evaluation. During the 1990s, aerial photographs and satellite images were first used and (digital elevation models (DEMs) were created from these sources [6]. Using a portable (global positioning system (GPS) coupled with geophysical imaging, particularly for methods acquiring electrical resistivity, has saved a large amount of work associated with identifying subsurface sediment bodies within a floodplain, which has considerably facilitated floodplain studies [7,8]. The performance of electrical resistivity imaging in floodplain studies has been demonstrated in previous works [9–12]. Since the beginning of the

21st century, precise digital terrain models produced from airborne laser scanning (LIDAR) data most commonly used for fluvial geomorphologic evaluation [13].

Studies on polluted floodplains are facilitated by pollution mapping that uses portable analytical instruments, including in situ analyses (without any sample pretreatment) [9,10]. In the last decade, portable analytical instruments, in particular those employing X-ray fluorescence (XRF), have reached quality levels suitable for geological research and environmental science monitoring [14]. In environmental geochemistry, portable XRF instruments are mainly used for quick pollution surveys and mapping [15–18]. Portable gamma and XRF spectrometers have also led to progress in detailed maps of pollution by radionuclides [9,19–22].

Portable XRF instruments offer many of advantages [14]: They have much lower operating costs, require much less demanding sample preparation compared to conventional laboratory analyses and can be used in situ in real time and results are immediately displayed. XRF can also be used to characterise sediment grain size, an essential factor in understanding floodplain sedimentary bodies [8,9]. In situ XRF analysis for high-density geochemical mapping opens new perspectives for analysing polluted soils and sediments.

There are two ways in which GIS approaches can contribute to pollution mapping in floodplains: (1) Geographical and geostatistical tools are essential for qualified imaging and interpretation of floodplain mapping results and (2) GIS systems greatly facilitate geomorphic interpretations by providing input materials, such as maps, vectorised past channel positions and digital elevation models for evaluating past and future floodplain evolution.

The Ploučnice River and its floodplain were polluted by local uranium mining (U-mining) from 1971–1989. This river has been studied since 2013 with the aim of identifying a relationship between the floodplain geomorphology and the spatial distribution of pollutants. We conducted several case studies in the localities shown in Figure 1. The most studied locality was the uranium pollution hotspot near Boreček village (acronym MH). In our first work [4], we used GIS for the characterisation of river channel shifts [23], laboratory XRF for chemical pollution analysis and electrical resistivity tomography (ERT) for imaging the floodplain fill. We later employed surface gamma activity mapping [21], more detailed ERT imaging and XRF analyses [9]; and finally, we also added dipole electromagnetic profiling (DEMP) and optically stimulated luminescence (OSL) for sediment dating [24]. Detailed geostatistical interpretation of the results of pollution mapping by XRF is demonstrated in this paper.

Spatiotemporal changes during the last two centuries in the Ploučnice River were studied between the towns of Stráž pod Ralskem and Česká Lípa [25]. GIS analysis was also used in other study areas: The second pollution hotspot south of Mimoň (acronym ES) [22,26]; the areas of “Žlutá značka” near Hradčany village (acronym AT1) [9,27] and “Sádlo”, west of Hradčany village (acronym AT2) [9]; the area in Veselí (acronym TV) [28]; the area “Martinova louka”, west of Hradčany village (acronym MS) [27,29]; and the area on the downstream bank of Česká Lípa town (acronym KK) [30]. Gamma activity mapping was also used in the study area ES [22,26], and ERT was also used in the areas AT1 and AT2 [9,31]. Sediment analyses with laboratory or field XRF were used in all studied areas. The first use of detailed XRF mapping in the floodplain was tested in the areas ES [26] and MS [27,29]. The methodology for geostatistical analysis of the results of XRF mapping was thoroughly examined in the areas TV [28] and KK [30].

We aim to show how GIS tools can aid in deciphering and understanding the internal structure of pollution hotspots, which we found in the studied floodplains, and how GIS and geomorphic evaluation can help to predict the risk of remobilisation of pollutants from these hotspots. This paper is focused on the geostatistical analysis of detailed XRF mapping in study areas MH, AT1 and MS, which were examined in the context of a master’s thesis [27]. This paper also demonstrates a combination of several methods: GIS for river channel shifts and geomorphology interpretation (MS and AT1), drone orthophoto mapping (MS), and surface gamma activity and subsurface XRF mapping (MS and AT1). We evaluated the hypothesis that these methods can enable us to understand why floodplain pollution

is deposited in spatially limited local hotspots and to evaluate whether the river channel dynamics may rework that pollution in the near future.

1.1. Study Areas

The Ploučnice River, a right bank tributary of the Labe (the Elbe) River, is 106 km long and drains 1194 km² of northern Bohemia, Czech Republic (Figure 1). The source rocks in the study area catchment are mainly Cretaceous sandstones, siltstones and marls; a minor proportion of sediment is derived from isolated bodies of Cenozoic volcanics present mainly in the form of individual hills with poor connection to the main stem. Mean discharge in Mimoň is 2.30 m³/s, and mean discharge in Česká Lípa is 4.90 m³/s. In the upper reach, downstream from Osečná, the flow gradient is up to 33.8 m/km, while only approximately 7 m/km in the lower stream west of Žandov. In the middle part of the flow, where the U-mining pollution was deposited, the slope decreases to approximately 0.8 m/km on average and to 0.6 m/km in the section between Hradčany and Česká Lípa [32].

In the studied areas, the Ploučnice River (Figure 1) is actively meandering with a valley gradient of only 0.6–1 m/km and a floodplain width of 100–200 m. The floodplain inundation is more or less annual; floods are currently caused mainly by summer local precipitation extremes. Frequent overbank flows precluded any intense agricultural floodplain use; in historical maps, crop fields were only located on terraces above the active floodplain, while the floodplain was used as pasture according to the Stable Cadastre map (1843). The fluvial deposits have lithologies ranging from fine gravel to mud in channels, sand to silt in lateral sediment bodies (bars) and mud (silt and clay) in floodplains.

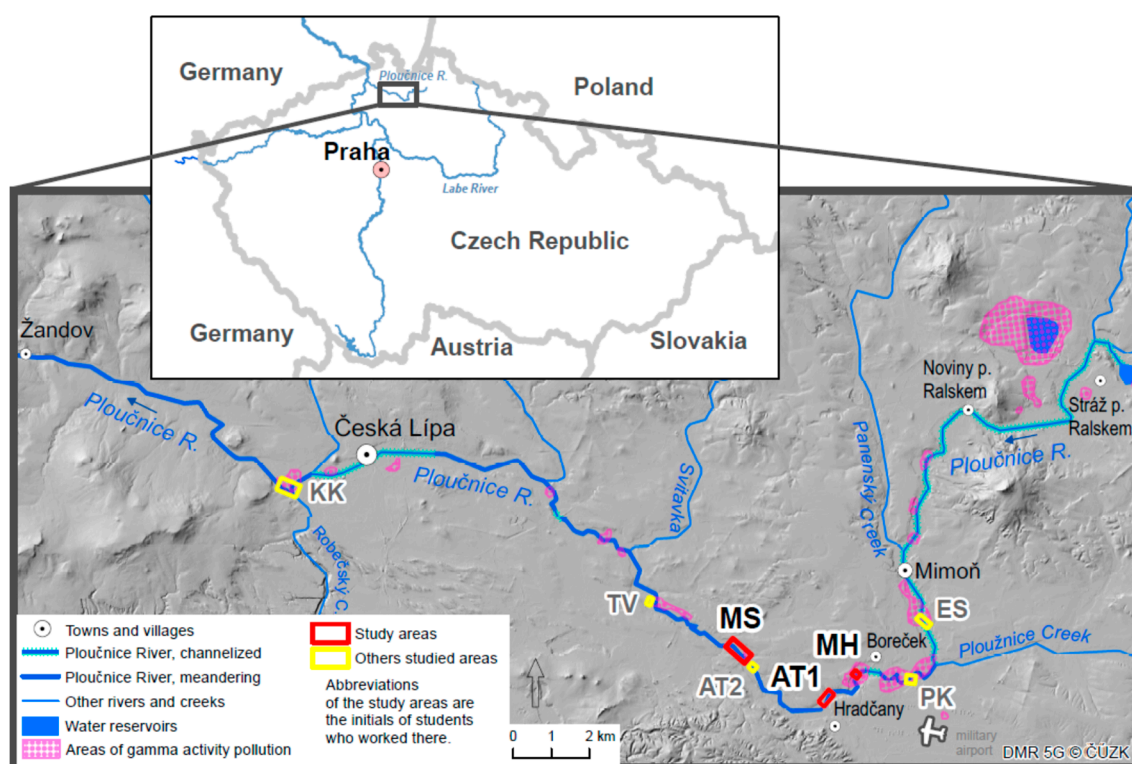


Figure 1. Map of the study areas in this research (red) and other studied areas (yellow). The acronyms of the study sites are the initials of students who worked there.

1.2. Pollution History of the Ploučnice River and Its Floodplain

Since the turn of the 19th and 20th century, local industrial enterprises, regional metallurgy and coal combustion [33] have caused diffuse pollution of the waste areas in the Czech Republic [11,34], including the Ploučnice floodplain [4,35]. Local industries in Panenský Creek, a right-side tributary of the Ploučnice River, have caused lead (Pb) and zinc (Zn) pollution [19,36]. Considerable pollution

of the Ploučnice River between the towns of Stráž pod Ralskem and Česká Lípa has been caused by U-mining, which started at the beginning of the 1960s and 1970s; pollution of the Ploučnice River system followed almost immediately [4,37–39]. The main pollutants from U-mining were radium (^{226}Ra), which is the major gamma emitting radionuclide in the polluted areas, uranium (U) and the less dangerous free acids, nickel (Ni) and Zn [4,19,38]. In summer 1981, extreme local precipitation caused a flood exceeding the 50-year river discharge (Q50) in the middle river reach. This flood was the worst flood that occurred in the second half of the 20th century. Hanslík [40] and Kühn [37] stated that this event caused the transport of a considerable number of particulate radionuclides from the mining area to the Ploučnice River.

The primary pollution from the mining area ended in the second half of the 1980s, when hydrodynamic barriers (a series of drill cores controlling underground fluid movements) stopped the overflow of solution from the in situ leaching fields to the underground mines. Almost simultaneously with this event, a sewage disposal plant was built and began operating. Soon after these measures, U-mining declined [38,39].

The results of an airborne survey by gamma spectrometry at a 250 m spatial resolution [41] revealed several pollution hotspots in the Ploučnice River floodplain between Mimoň and Česká Lípa (Figure 1). In the early 1990s, floodplain sediments were cored and analysed for one hotspot [19]; and ten years later, Ploučnice channel sediments were analysed [36,42], but the importance of fluvial processes in pollutant deposition and spread was not discussed in these early works. Thus far, a systematic study of the floodplain has been initiated to understand and interpret the pollutant distribution there and the reasons for the existence of contrasting gamma activity hotspots [4,9,21,24].

2. Materials and Methods

2.1. GIS Data Collection and Processing

To understand the floodplain development and pollution heterogeneity, we collected archival materials of all study areas, information on pollution history and past floods and old maps and aerial photographs (Figure 2).

Datasets for the GIS analysis were purchased from the Czech Office for Surveying, Mapping and Cadastre (Imperial Obligatory Imprints of the Stable Cadastre, archive orthophoto from 1999 to recent orthophoto from 2015; © ČÚZK), the Geoinformatics Laboratory at J.E. Purkyně University (2nd Austrian Military Survey, 1836–1852; © UJEP), and the Military Geographic and Hydrometeorology Office (aerial photos from 1938 through 1992; © MO ČR). Aerial photos from 1938, 1953, 1976, 1982 and 1992 were orthorectified in ERDAS LPS 2013 (Hexagon Geospatial, Madison, WI, USA) [23], and spatiotemporal changes in the Ploučnice River were analysed using ArcGIS software (Esri, Redlands, CA, USA). The near feature and intersect analysis identified river areas where the channel was straightened or altered [23,25].

The Digital Terrain Model of the Czech Republic of the 5th generation (DMR 5G; © ČÚZK) was based on data obtained by aerial laser scanning the Czech Republic between 2009 and 2013. The DMR_5G represents an image of natural or man-modified terrain in digital form as the heights of discrete points in a triangulated irregular network (TIN) with a total mean error of 0.18 m height in open terrain and 0.3 m in forested terrain [43]. The laser scanning dataset (DTM) from 2010 was used to create a three-dimensional model (TIN) for visualisation and a raster digital terrain model with 0.5 m resolution for surface analysis. Based on slope, aspect and visibility maps, a detailed geomorphologic analysis of the study areas was performed. The TIN datasets are also freely available online with a 2 m resolution: <https://ags.cuzk.cz/dmr/>.

The MS study area was also scanned with a drone from a height of 50 m (Figure 3B). A micro-UAV system SteadiDrone EI8HT with a Sigma 35 mm f/1.4 DG HSM Nikon lens and stabilisation device (gimbal) was used. More than 350 images were collected. The images were orthorectified in Agisoft PhotoScan software (St. Peterburg, Russia) with a 4 cm resolution.

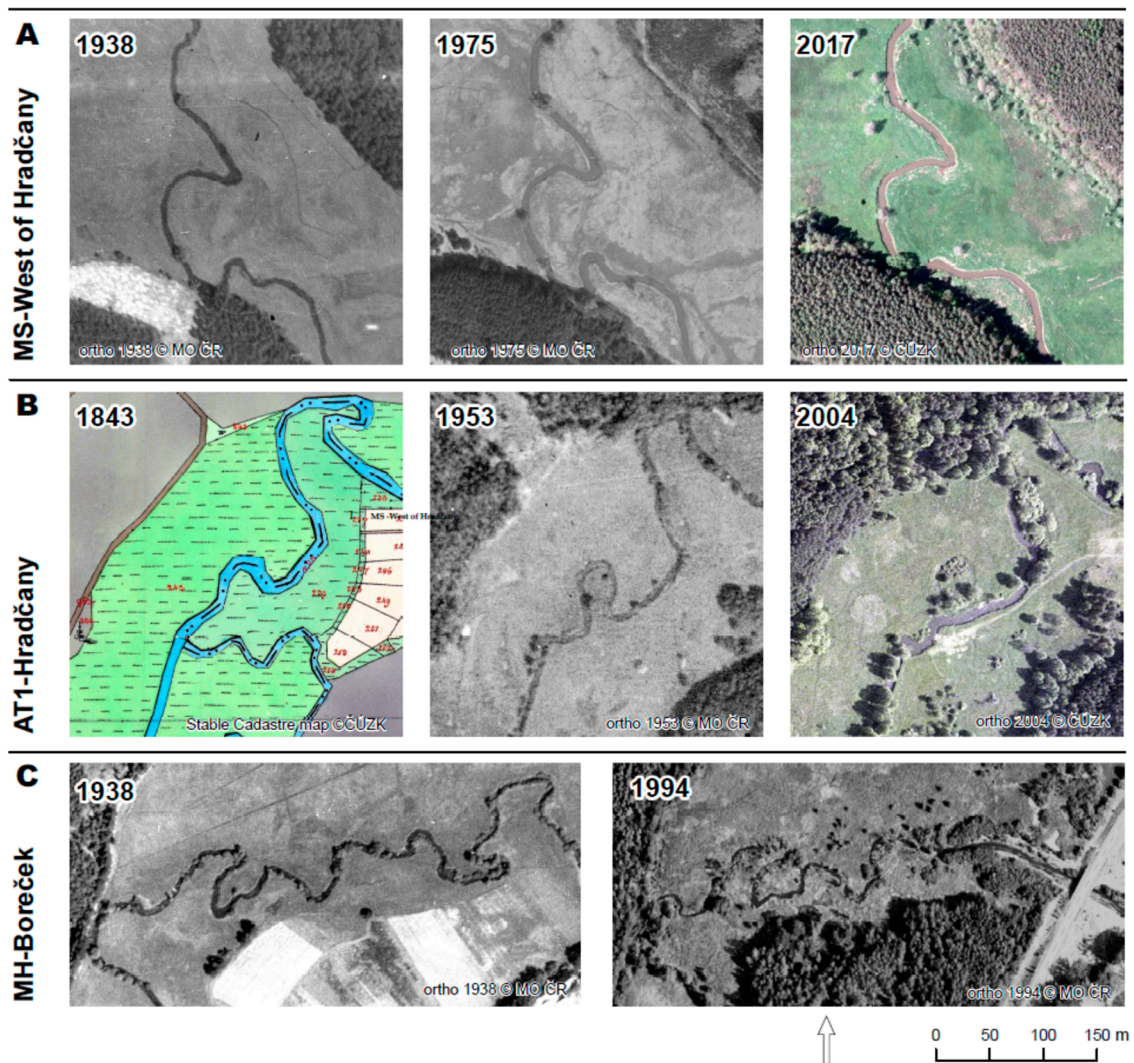


Figure 2. Stable Cadastre maps and archive orthophotos of the study areas.

River channels from different years were vectorised as polylines. The channel parameters (length, stream gradient and sinuosity [44]) and changes in the Ploučnice River (straightening, lateral shifts, meander evolution, and eventual meander cut-offs) were analysed using spatial analysis. Data processing, analysis and visualisation were conducted in ArcGIS Desktop 10.5 with the 3D Analyst extension.

2.2. Pollution Mapping

Using GIS analysis, hotspots of river change were identified, and non-invasive geophysical imaging began in these areas. We also used a historical low-resolution map (Figure 3A), which was based on aerial gamma spectrometry and was performed with a handheld gamma spectrometer GT-30 (Georadis, Brno, Czech Republic) in 2005 [41]. Spatial resolution of the interpolated gamma activity raster was approximately 25 m, but the distance between individual neighbouring measurement points was approximately 250 m. Based on the resulting maps, floodplain sediments were analysed in three study areas by non-destructive in situ methods. Floodplain contamination was detected mainly by two portable (handheld) XRF instruments. Pollution mapping requires sufficient density analyses, because pollution hotspots may be localised to very narrow strips in former channel areas, presently filling with sediment [28]. Whenever pollution has been covered by less polluted sediments since the pollution climax, XRF cannot be performed on the top surface of the floodplain strata but must be

applied to shallow sediment cores [24]. Surface gamma activity can also be acquired from pollution covered by up to ca. 0.2 m of less polluted strata; such layers can accumulate over more than 50 years in a floodplain (mean deposition rate of overbank fine sediments in floodplains is on the order of mm/y) or possibly sooner in deeper underlying surfaces near active channels.

To measure the total surface gamma activity (^{226}Ra was the main target nuclide), we used a gamma-spectrometer DISA 400A or GT-30 equipped with a 1024-channel NaI (T1) detector operating in the energy range between 30 keV and 3 MeV. For mapping, we used the “survey” feature set to monitor the total gamma radiation at waist level to hasten the process. The gamma activity survey mainly collects information from the top strata to a depth of ca. 0.2 m, while thicker sediment cover over pollution would attenuate surface activity. For the MS area, we collected more than 1500 data points (Figure 3C). The results were interpolated and visualised with Surfer 8 (Golden Software, Golden, CO, USA).

We also used the portable XRF instrument DELTA Premium by Olympus Innov-X, which provides rapid analysis of more than 30 elements, such as pollutants (Ba, Ni, Pb, U and Zn) and grain-size sensitive lithogenic elements (Al, Fe, Rb, Si, and Zr). Most chemical elements (both polluting and lithogenic) in chemically mature sediments are grain-size sensitive. For example, the aluminium to silicon (Al/Si) ratio is considered a “surrogate” for grain size of fluvial sediments [45–47], because, in mature sediments, this ratio increases with a growing percentage of clay fraction (usually dominated by aluminosilicate clay minerals) at the expense of sand (usually dominated by quartz). Conversely, the zirconium to rubidium (Zr/Rb) ratio in sediments is proportional to coarser particle content, in particular coarse silt and the finest sand [48,49], because Zr is mainly carried by zircon crystals with a typical grain size of 0.05 to 0.1 mm, and because in mature sediments, Rb occurs mainly in finer clay mineral particles. XRF is suitable for analysis of both pollutants (risk elements) and lithogenic elements, including those whose determination by common methods, such as dissolution in mineral acids and ICP spectrometry, is not possible, e.g., Si. The levels of the lithogenic element concentrations in sediments are required for grain-size correction of the risk element concentrations to distinguish pollution from natural variability [4,45,50–53]. The simplest grain-size correction is geochemical normalisation, e.g., expression of pollution extent as a ratio of a risk element to a lithogenic element, such as Al, iron (Fe), Rb, and titanium (Ti) [54], which also corrects non-ideality of in situ XRF spectra acquisition [55].

One XRF shot (point measurement) required 70 seconds and is thus several orders of magnitude faster than lab sample processing for analysis by atomic absorption spectrometry (AAS) or inductively coupled plasma (ICP with atomic spectrometries). In the MS area, more than 450 XRF point analyses were collected (Figure 3D). The major limitations of the XRF analysis include an analytical signal penetration depth of less than 1 mm and the influence of textural inhomogeneity of native sediments. The latter is mostly reduced by using geochemical normalisation (see the preceding paragraph).

All the instruments can be connected to GPS to obtain geographic coordinates. Acquired data can be visualised in GIS. Figure 3 shows data used for the MS study area. The drone mapping lasted approximately about two hours, the gamma radiation mapping approximately about seven hours, and the XRF mapping approximately about 25 h.

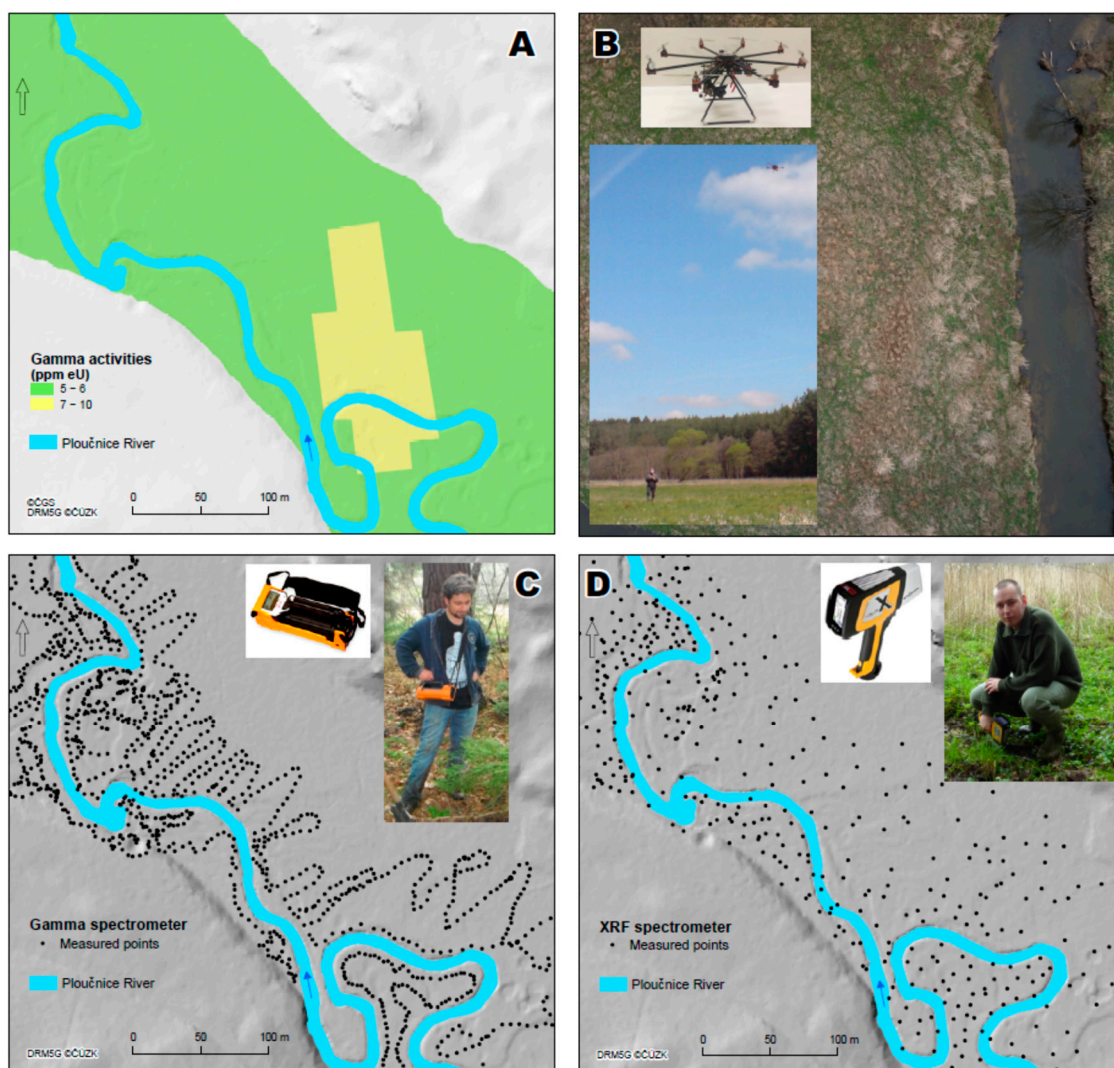


Figure 3. Mapping instruments in the MS-West of Hradčany study area: Low resolution gamma activity survey (A), drone and detail of a high-resolution image (B), gamma spectrometer and measuring points (C), and X-ray fluorescence (XRF) spectrometer and measuring points (D).

2.3. Geostatistical Analysis

We performed a geostatistical interpolation in ArcMap 10.6 software with the Geostatistical Analyst extension to create statistically valid predictions of surface gamma activity, concentrations of Zn and U and relative ratios of selected elements. The data were initially transformed using normal score transformation. This data transformation is crucial for the kriging interpolation, as this method assumes normally or at least symmetrically distributed data. Long upper tails in the distributions of positively skewed data inflate variances and distort variograms [56]. Like many other environmental variables, pollution datasets are positively skewed, sometimes strongly, due to high values (outliers and/or extremes) present in pollution hotspots. Commonly applied logarithmic transformation cannot be used, as measured XRF concentration often has a zero value (below the determination limit). Thus, normal score transformation (NST) is a good alternative to logarithmic transformation. The NST is designed to transform datasets so that they closely resemble a standard normal distribution by ranking the values from lowest to highest and matching these ranks to equivalent ranks generated from a normal distribution [57]. ArcMap 10.6 software allows NST for simple kriging only [57], which is one of the arguments for choosing this type of kriging. The mean measured values are assumed to be constant over the whole domain; thus, simple kriging (SK) was chosen as the appropriate interpolation

method. The estimated means (Table 1) were calculated as the average of the data [58]. The means of U, the U/Fe ratio, Zn, and the Zn/Fe ratio are close to zero, the means of the Al/Si ratio are between 0.2 and 0.3 and the means of the Zr/Rb ratio are approximately 5 in all three study areas.

Table 1. Parameters of geostatistical interpolation (simple kriging).

MS-West of Hradčany						
XRF Value	Estimated Mean	Variogram Function	Nugget	Nugget-to-Sill Ratio (%)	Major Range	RMSPE
U	0.002	Spherical	0.650	57	41.455	0.903
U/Fe	0.000	Circular	0.864	92	41.316	1.068
Zn	0.019	Spherical	0.519	51	55.936	1.035
Zn/Fe	0.011	Circular	0.761	76	27.933	1.004
Al/Si	0.303	J-Bessel	0.381	38	113.408	0.977
Zr/Rb	4.903	Circular	0.237	27	58.651	1.065
AT1-Hradčany						
XRF Value	Estimated Mean	Variogram Function	Nugget	Nugget-to-Sill Ratio (%)	Major Range	RMSPE
U	0.002	Circular	0.490	46	58.249	1.007
U/Fe	0.001	Circular	0.469	45	51.421	0.915
Zn	0.016	Circular	0.578	55	26.673	0.913
Zn/Fe	0.008	Spherical	0.370	39	26.456	0.941
Al/Si	0.210	Spherical	0.377	39	50.921	0.950
Zr/Rb	5.128	J-Bessel	0.405	41	83.895	0.894
MH-Boreček						
XRF Value	Estimated Mean	Variogram Function	Nugget	Nugget-to-Sill Ratio (%)	Major Range	RMSPE
U	0.003	J-Bessel	0	0	15.472	1.020
U/Fe	0.001	Circular	0	0	12.495	0.958
Zn	0.040	Circular	0.186	15	22.645	1.007
Zn/Fe	0.016	Exponential	0	0	12.739	1.116
Al/Si	0.203	Circular	0.001	0	73.179	1.002
Zr/Rb	4.866	J-Bessel	0.162	17	43.458	0.982

Kriging is a local predictor, and only the nearest few points to the target point carry significant weight [56]. In the next step, an optimal experimental variogram function (see Figure 4) was chosen from a group of functions (stable, exponential, spherical, circular or J-Bessel), as the function that provided the closest value to the root mean square standardised prediction error (RMSPE). The RMSPE value calculated using cross-validation techniques (in our case, the leave-one-out method) can be used to choose the best variogram model from the candidates [59]. Detailed results of selected variogram functions and estimated parameters are shown in Table 1. As the RMSPE values are close to one in the majority of cases, the final interpolations produced good pollution maps.

Samples separated by a distance larger than the range are spatially independent because the estimated semivariance of differences is invariant with the sample separation distance. The estimated major range provides information regarding the size of a search window used in the spatial interpolation methods [60]. According to [56], the minimum number of points in the interpolation neighbourhood was set to 7 and the maximum was set to 25. Nugget is the residual reflecting the variance of sampling errors and the spatial variance at a shorter distance than the minimum sample spacing [59].

Spatial dependency is commonly accessed in terms of a nugget-to-sill ratio expressed as a percentage [61]. In this respect, a low ratio (less than 25%) was found for all XRF values in MH (Boreček), and this finding indicates that a large part of the variance is introduced spatially, implying a strong spatial dependency of the variable. A high ratio (more than 75%) was found only with the

U/Fe ratio in MS area, and this result often indicates weak spatial dependency at the present sampling resolution. The degree of kriging smoothing depends on the nugget-to-sill ratio. The larger the ratio is, the greater is the smoothing (kriging tends to underestimate large values and overestimate small values) [56]. From this perspective, the smoothing of all XRF values (except the U/Fe and Zn/Fe ratios in MS area) is relatively small, which is an important property for mapping pollution hotspots.

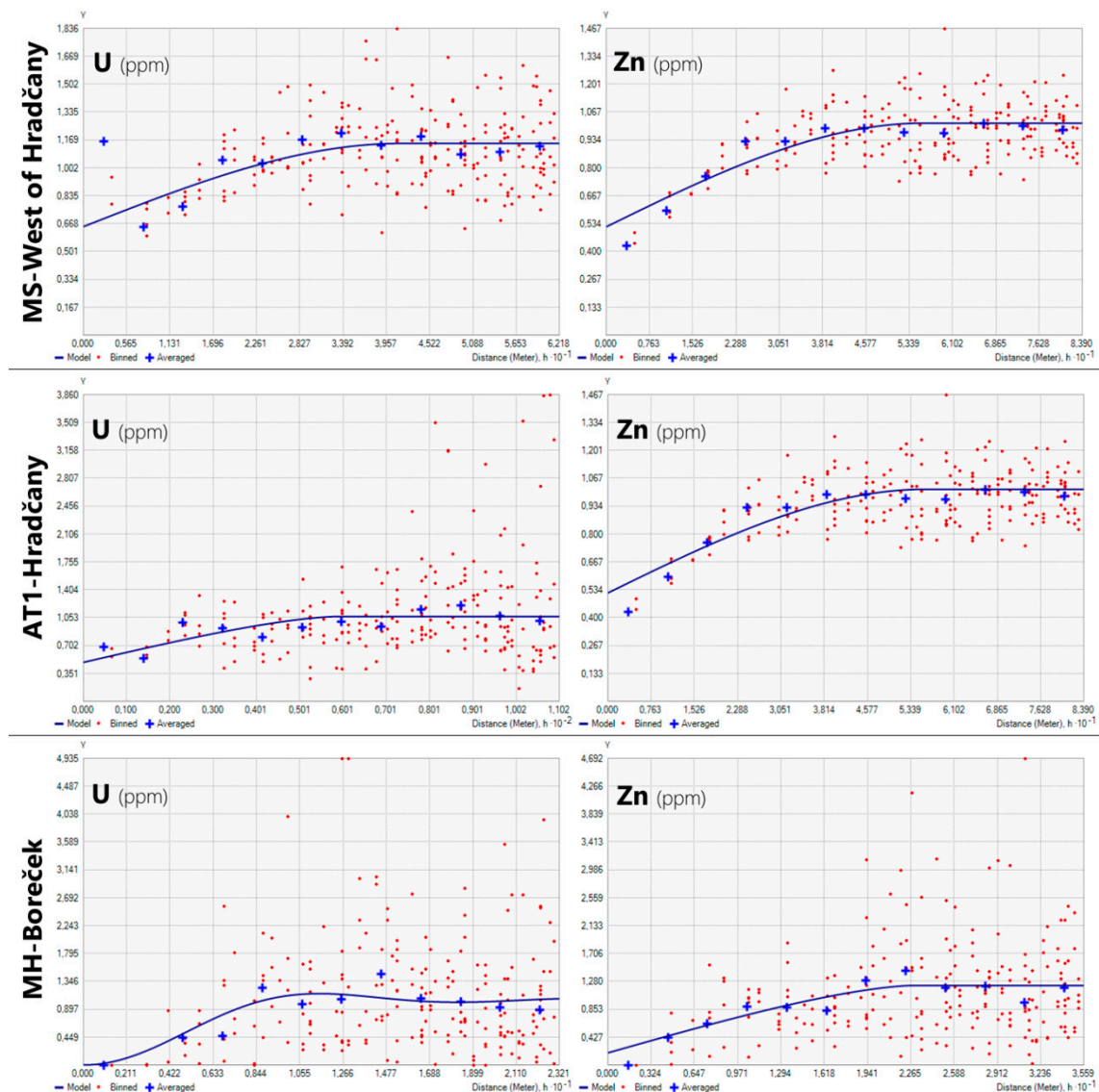


Figure 4. Estimated optimal variogram functions (blue lines) for U (left panels) and Zn (right panels) in the study areas.

3. Results

3.1. River Dynamics and Engineering

The channel position of the Ploučnice River was analysed using GIS tools. To understand floodplain development, old maps, aerial photographs and DEMs were used. The total channel length between Stráž pod Ralskem and Žandov (Figure 1) decreased from 76.5 km at the time of the 2nd Austrian Military Survey (1836–1852) to 66 km in 2011. The main changes in the river channel have been caused by channel straightening carried out to prevent flood damages and by U-mining pollution between the towns of Stráž pod Ralskem and Mimoň. Channel engineering was also substantial in Boreček village, due to the construction of a new road bridge [23] and along the river stretch around

Česká Lípa town [25]. Due to this channel straightening, the average stream sinuosity decreased from 2.56 to 2.22 and the gradient increased by 0.02 m/km.

Natural meandering in the middle river reach during the U-mining period took place in the entire river stretch between the towns of Mimoň and Česká Lípa. Lateral channel instability is an important characteristic of the former middle river reach. The floodplain deposits of the Ploučnice River are sandy to silty, which reflects the catchment lithology. Consequently, the river channel has shown considerable lateral shifts in the order of 10^0 to 10^1 m and several meander cut-offs, one of which is shown in Figure 5B. The lateral shifts in the river channel have reworked sediments and thus continuously created new sediment accommodation space (see Figure 5A). An overview of the changes in the channel positions from aerial photos in the study areas is shown in Figures 2 and 5.

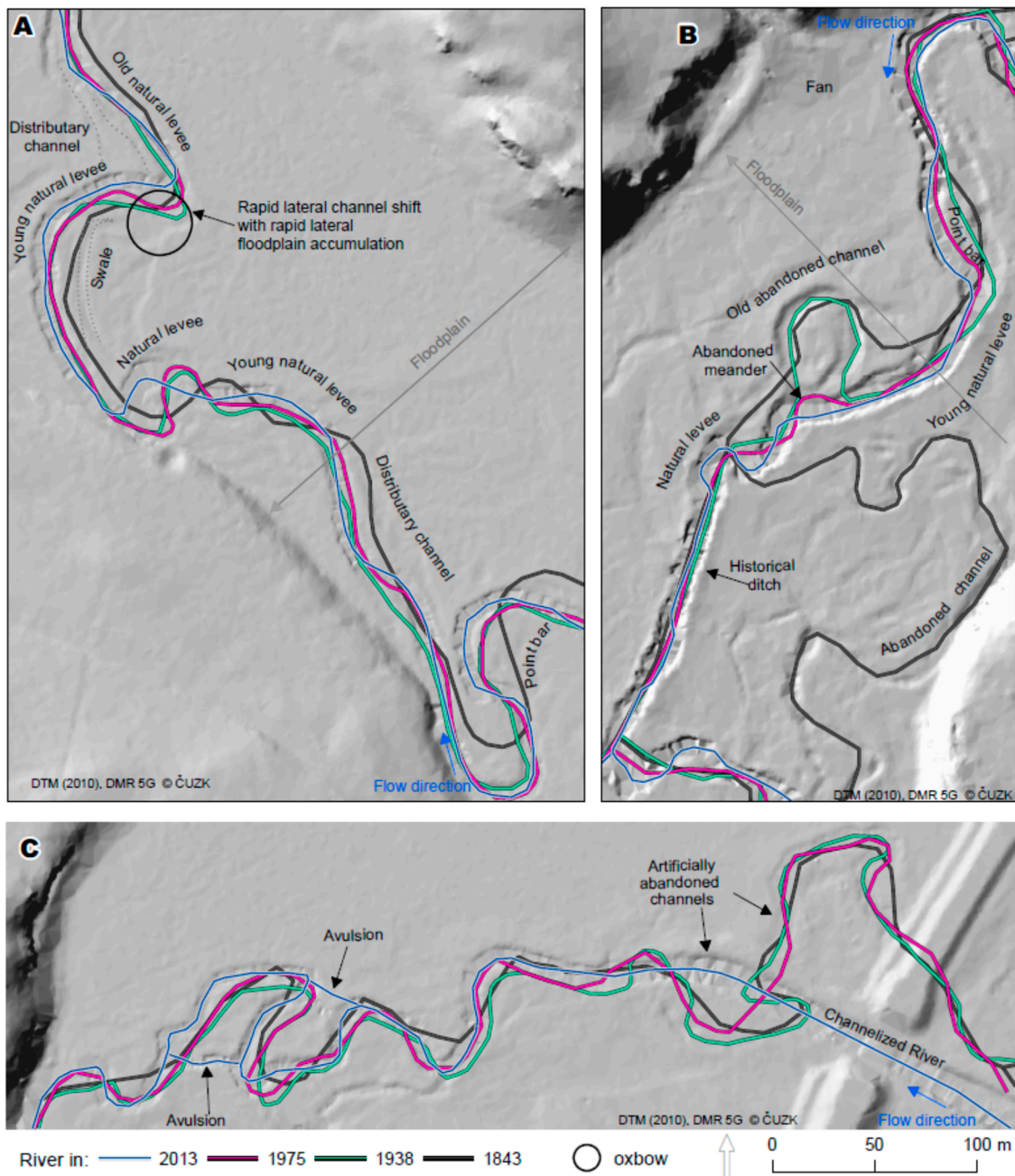


Figure 5. Historical channel positions and interpreted geomorphologic features in the study areas: (A) MS-West of Hradčany, (B) AT1-Hradčany, and (C) MH-Boreček.

Our study areas show examples of fluvial dynamics associated with human activities. The AT1 study area (Figure 5B) is situated in an area with an example of historical human interference with the river system. A ditch for a mill downstream of the AT1 area was constructed at the end of the 18th century (Figure 5B); the new ditch and original channel coexisted in the Stable Cadastre map (Figure 2B). In the period between drawing the Stable Cadastre map and the first orthophoto in 1938, the river was completely redirected to this ditch and the original natural channel was completely abandoned (Figures 2B and 5B). After that human-generated avulsion, a meander developed just upstream from the avulsion point and was abandoned in the second half of the 20th century (Figure 5B).

The MH study area is located downstream of the road bridge constructed between 1982 and 1994 (Figure 2C). The river channel was shifted and straightened below the bridge (Figure 5C) and two small-scale avulsions then shortened the river course downstream, probably as a direct result of the increased channel gradient.

In all study areas, deposition in point bars was quite extensive. Point bars are shown in Figure 5A,B as slightly lower lying surfaces elongated along laterally shifting channels. The extent of point bars can actually be estimated from the shifts in historical channel positions visible in Figures 2 and 5. The areas with recent lateral channel shifts thus definitely accommodated considerable sediment volumes from the U-mining period.

3.2. Pollution and Lithological Mapping

3.2.1. Pollution Mapping in the MS-West of Hradčany Study Area

The MS study area (Figure 6) is the largest of the three areas that we subjected to surface gamma activity and geochemical mapping in the Ploučnice floodplain. The area is more remote from the U-mining location than the hotspot in Boreček (MH) studied previously [4,9,19,24], as well as far from any river engineering measures. The MS area seemed unpolluted or only very weakly polluted in the low-resolution airborne gamma radiation survey (Figure 3A); however, smaller but considerably polluted areas were found at this site by our own detailed survey (Figure 6B).

The main local pollution hotspot in the MS area was revealed by both the XRF and gamma activity surveys near a location of channel reorganisation during the U-mining period (Figures 6 and 7, near the pictogram of a fallen tree and just upstream from this location). The river channel in this location shifted laterally according to historical aerial photographs and led to in-channel deposition between 1953 and 2008. A small oxbow lake is still on site, marked by the circle in Figures 5–7, and; therefore, the surface topography clearly reveals those former channel shifts up until now. In a very nearby downstream location, remnants of a tree trunk base were found on the right bank, while the trunk fragments are still visible in the channel, and branches from the top of the tree crown lay on the left bank. The position of the fallen tree is marked in Figure 6; the detailed tree remnants are shown in the UAV photograph in Figure 6A. The trunk in the channel has inevitably become a hindrance to the water flow and has therefore enhanced overbank flow and sediment deposition in the proximal floodplain during floods. This main pollution hotspot is clearly discernible by elevated concentrations of Zn and U (Figure 6C,E), as well as the Zn/Fe ratio near the fallen tree (Figure 6F). The polluted sediment at this location has a larger mean grain size (lower Al/Si and higher Zr/Rb ratios, see Figure 7) and has accumulated on an elevated ridge along the channel. In other words, the pollution hotspot in the MS area is situated on top of a natural levee.

At other sites in the MS study area, the XRF and gamma activity maps produced remarkably different outputs. Several gamma activity hotspots were found in the meander belt, i.e., tightly along the river channel in locations with recent lateral channel shifts (Figure 6B), where only medium surface concentrations of chemical pollutants (U and Zn) were found with XRF mapping (Figure 6C–F). Only in one case is the same hotspot visible in both gamma activity map and the Zn/Fe ratio map (Figure 6F). The gamma activity hotspots (dark red areas in Figure 6B) are clearly identical with the point bars, i.e., in-channel deposits in locations where the river channel was systematically (single-directionally)

laterally shifted during the U-mining period (note the changing historical position of the river channel, shown in Figures 2 and 5–7).

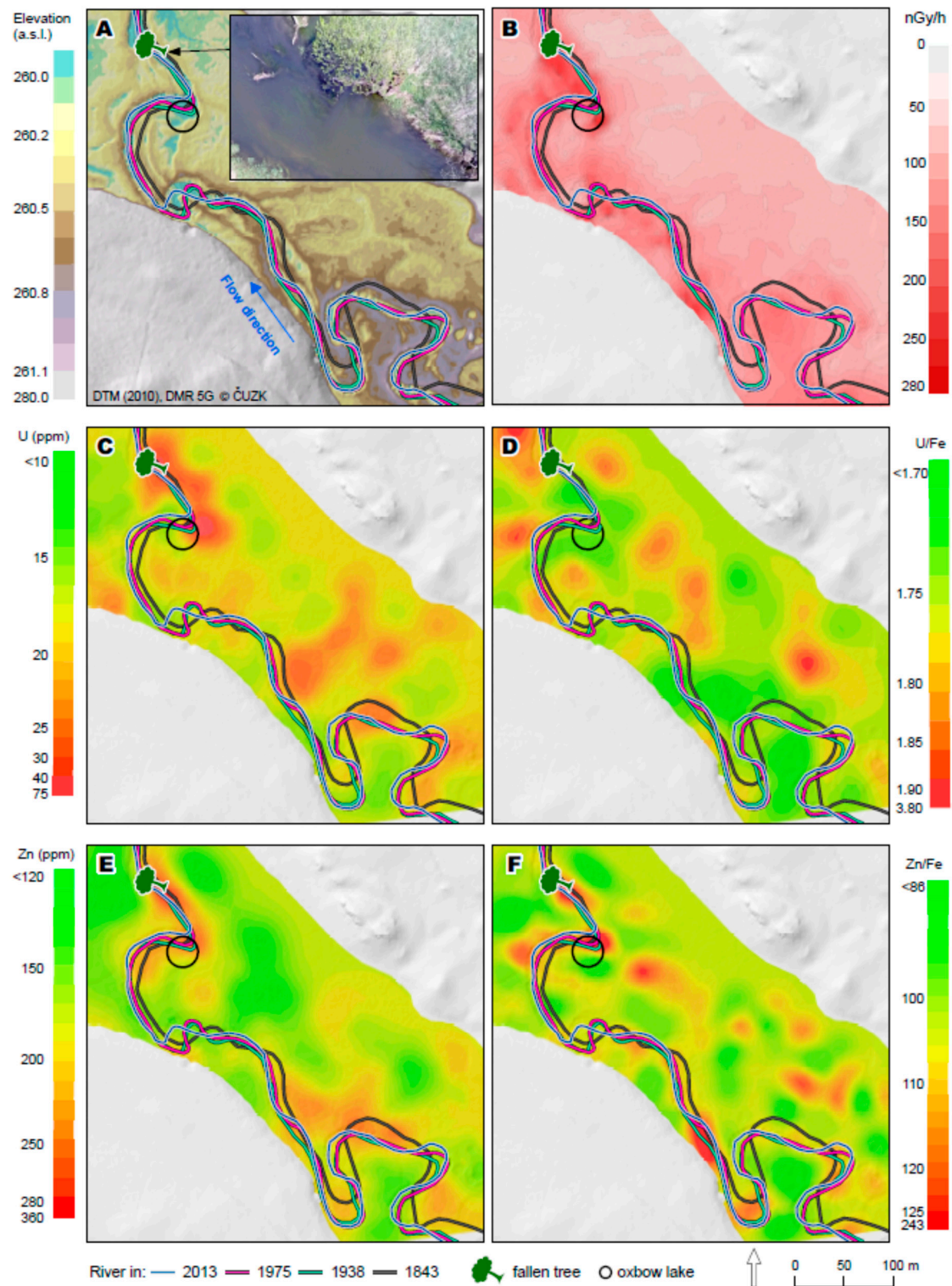


Figure 6. The MS-West of Hradčany study area. Digital terrain model and an aerial photograph (panel A), gamma activity map (panel B) and XRF maps of U (panel C), the U/Fe ratio (panel D), Zn (panel E) and the Zn/Fe ratio (panel F). Historical channel positions are also shown. Inset in panel A shows an aerial photograph of the tree remnant in the channel.

This systematic channel movement facilitated deposition in the channel belt, as well as the preservation of these deposits. The reason for the discrepancy between gamma and XRF mapping is clear: The deposition in point bars is much faster (typically several centimetres per year) than in the distal floodplain (typically several millimetres per year); and hence, the historical uranium pollution in the bars was buried between the 1990s and the present time by a layer of less polluted (younger) sediments too thick to reveal pollution by surface XRF analysis. The fact that the gamma activity hotspots along the river channel are truly point bars is also obvious from their coarser grain size compared to the floodplain, i.e., lower Al/Si and higher Zr/Rb ratios (Figure 7A,B, respectively). Coarser sediments are also located on natural levees around channel bends; the blue arrows in Figure 7 indicate tangential directions of preferential overbank export of these coarser clastics. Some of these natural levees, in particular those formed during the U-mining period, also show elevated surface gamma activity.

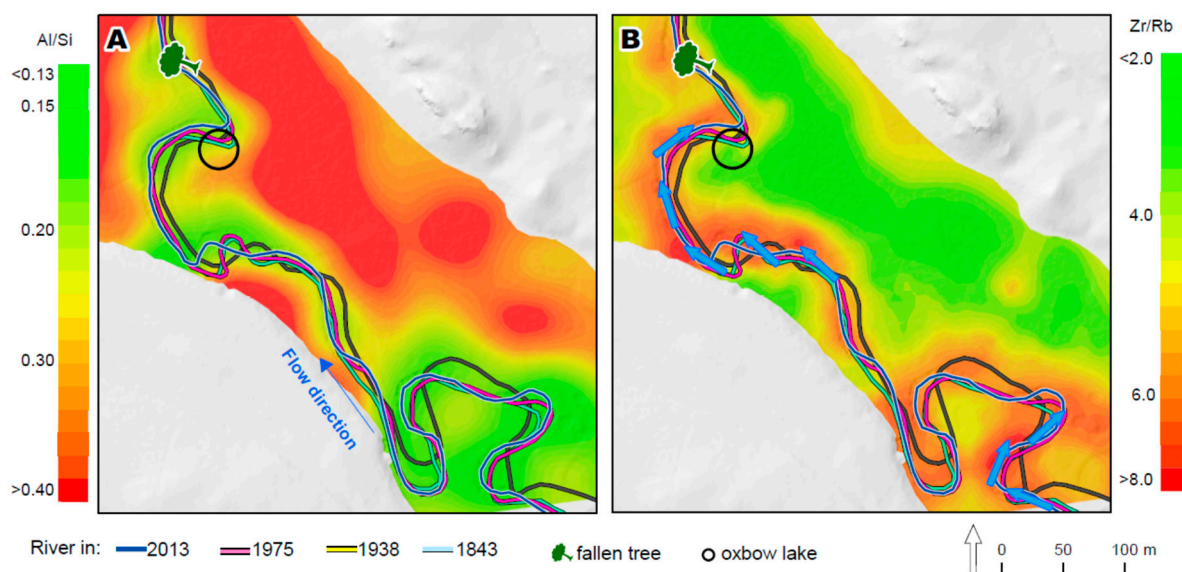


Figure 7. Maps of Al/Si (A) and Zr/Rb (B) ratios in the MS-West of Hradčany study area. Blue arrows indicate enhanced transport paths of overbank clastics as extrapolation of flow directions; they point to study areas with coarser overbank sediments, where gamma activity and XRF mapping produced markedly different results.

The MS study area is notable for large differences in sediment lithology, i.e., mean grain size, documented by variable Al/Si and Zr/Rb patterns. Normalisation of the polluting element concentrations to the lithogenic element, here Fe, in XRF maps from the MS area nearly levelled out the variance in U concentrations in the study area: Comparing Figure 6C (raw U concentrations) and Figure 6D (U/Fe normalised values) shows much lower variance in the corresponding colour scales in the latter figure. The reason is that the main driver of elevated surface U concentrations was the mean sediment grain size: Both U and Fe are elevated in finer sediments. In contrast, even after normalisation, Zn pollution reaches a maximum in the local pollution hotspots according to the gamma activity map discussed above (Figure 6E,F), although normalisation also considerably decreased the total variance of the pollution extent. The reason for better correlation of the surface Zn/Fe ratio and gamma activity than of the surface U/Fe ratio and gamma activity is currently unclear; obviously, both the surface Zn/Fe ratio and gamma activity show the locations in floodplains where pollutants were preferentially deposited.

3.2.2. Pollution Mapping in the AT1–Hradčany Study Area

Similarly, to the MS study area, part of the pollution is concentrated in a point bar in the AT1 study area. This contamination is visualised by gamma-activity, U, the U/Fe ratio, Zn and the Zn/Fe

ratio maxima in the top right areas of panels B through F in Figure 8. There are two differences in the AT1 study area compared to the MS study area: (1) Levee deposits around convex river banks are not highly polluted and (2) the interpolated pollution images are similar for both raw (U and Zn concentrations and gamma activity) and normalised concentrations (U/Fe and Zn/Fe ratios), showing the less important effect of sediment grain size, as is clear from similar pollution maxima in the individual panels in Figure 8.

The AT1 study area is particular for the presence of a regular meander loop abandoned by a natural neck cut-off just before the U-mining period. This cut-off meander was subsequently filled with sediments during the mining period (Figures 2B and 5B). The location of a ring-shaped pollution maximum is visible in the centre of Figure 8B–D,F.

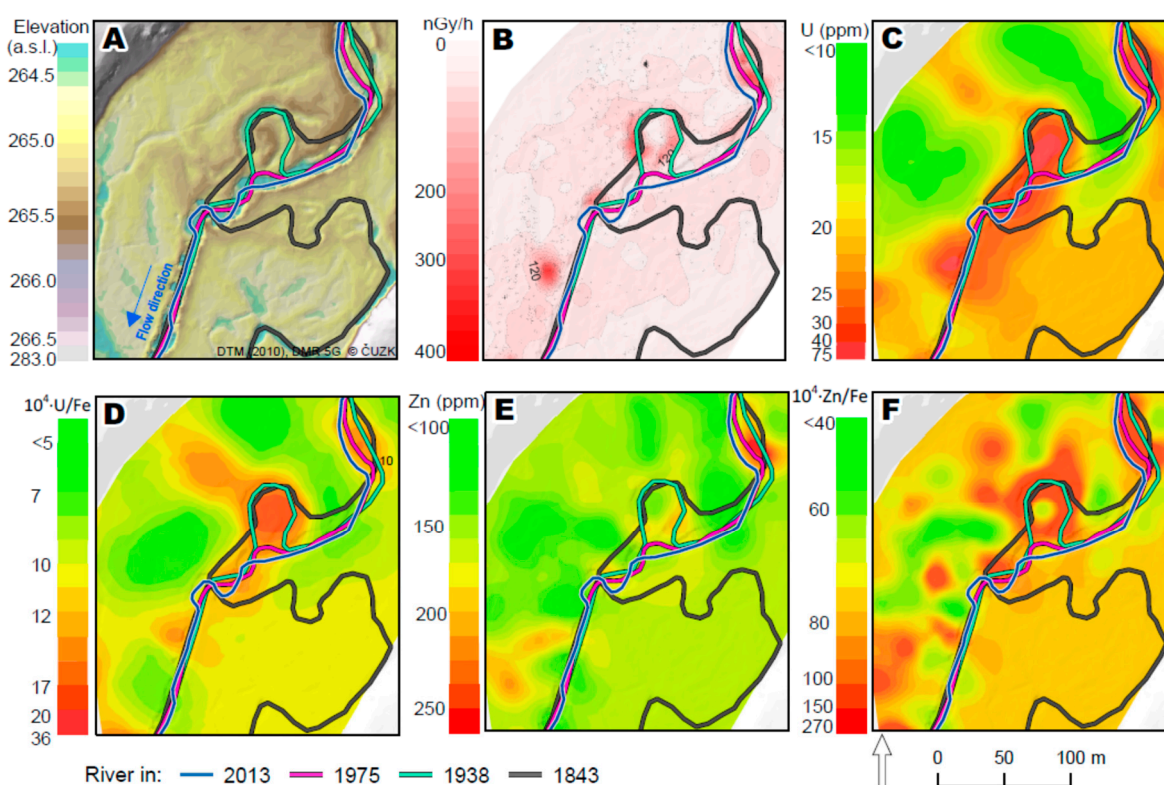


Figure 8. The AT1-Hradčany study area. Digital terrain model (panel A), gamma activity map (panel B), XRF maps of U (panel C) and the U/Fe ratio (panel D), and XRF maps of Zn (panel E) and the Zn/Fe ratio (panel F). Historical channel positions are also shown.

3.2.3. Pollution Mapping in the MH–Boreček Study Area

The MH study area (Figure 9) has the smallest extent among all the pollution hotspots that we have studied thus far. Another peculiarity of the MH study area is, however, its complexity, which is obvious from the most complex internal structure of surface gamma activity maxima (Figure 9B) and U and Zn distribution (Figure 9C–F), particularly with respect to the lack of channel reorganisations in historical maps and orthophotos from the mining period (Figure 2C). The floodplain topography of the mapped area is rather uniform (Figure 9A) and has no obvious apparent relation to the complexity of the pollution hotspot. There may not normally be a need to decipher the structure of such a complex and small area; however, this location showed the highest surface gamma activity (Figure 9B) and concentrations of Zn and ratios of Zn/Fe (Figure 9E,F, respectively) among the study areas and was lacking in straightforward geomorphic interpretations.

The U and U/Fe ratio maxima in the top right part areas of Figure 9C,D can be attributed to the levee around the active channel. These maxima did not reflect a specific lithology of the levee sediments, as the U and U/Fe ratio maps are nearly the same in this particular location. The pollution

maxima in the U and Zn geochemical maps of U and Zn do not overlap (comparing Figure 9C,E), but at least the gamma activity maxima (Figure 9B) overlaps with the U and U/Fe ratio maxima (Figure 9C,D, respectively) as can be expected for U-mining related pollution. The MH study area documents that each segment of floodplain impacted by mining shows site-specific features. Notably, the MH area underwent the most relevant anthropogenic impacts to the Ploučnice River system from of the three study areas, as described in Section 3.1. This aspect will be considered in the Discussion.

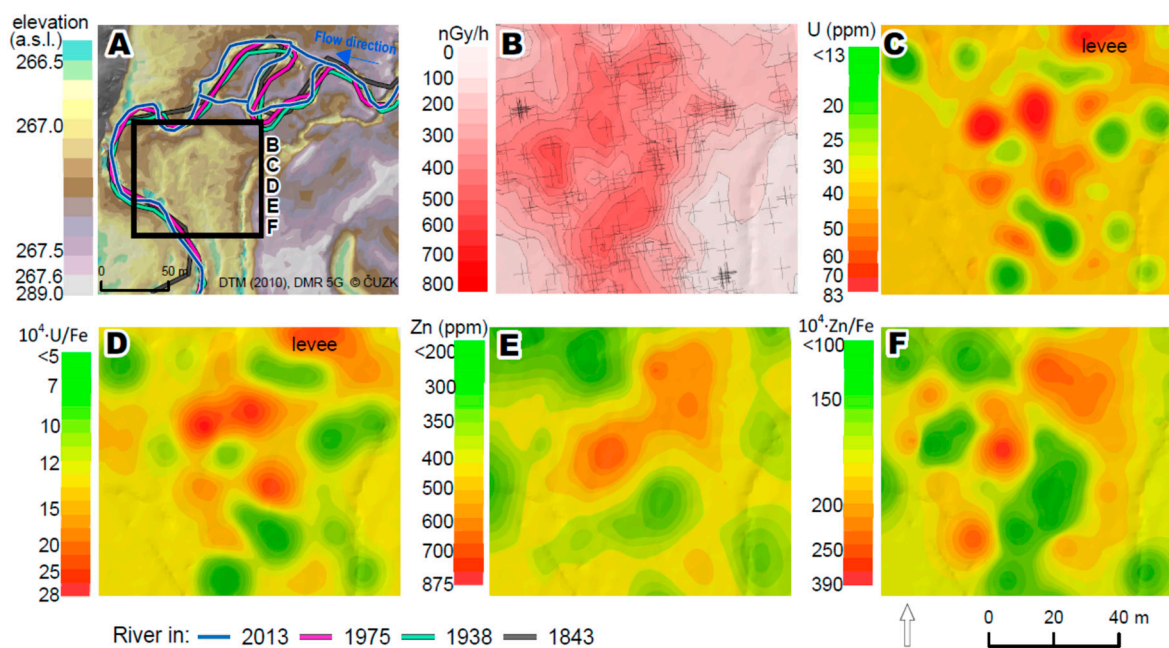


Figure 9. The MH–Boreček study area. Digital terrain model (panel A), gamma activity map (panel B), XRF maps of U (panel C) and the U/Fe ratio (panel D), and XRF maps of Zn (panel E) and the Zn/Fe ratio (panel F). Historical channel positions are also shown.

4. Discussion

The in situ analysis by handheld XRF instruments is directly applicable to pollution mapping in floodplains (Figures 6, 8 and 9), although due to “native” water content, the as yet obtained element concentrations represent only 45–70% of the conventional total content on a dry sample basis. Such an effect of the water content aligns with previous observations by researchers who performed an analysis of native sediment samples without pretreatment [17,62,63]. This inherent effect of field analysis of native samples can be corrected by geochemical normalisation, i.e., expression of pollutant concentrations as relative ratios, such as the U/Fe and Zn/Fe ratios used in our work. The overall advantages of geochemical normalisation are well known [54]. With in situ XRF, it is also easy to perform lithological mapping of the floodplain surface, i.e., imaging of a proxy for the mean sediment grain size directly in the field (Figure 7). Lithological mapping is essential for distinguishing individual sediment facies, such as deposits of point bars, levees and overbank floods, the last being the finest (having the highest Al/Si and the lowest Zr/Rb ratios). In some locations, these lithological differences controlled pollutant distribution, which is visible from the striking differences between raw and normalised pollutant concentrations.

If pollution hotspots are associated with geomorphic features (Figure 2), each sedimentary unit must be covered by a sufficient number of analyses to be visualised by kriging. Pollution mapping is most economic if the surface topography is recognised before finishing instrumental analysis in the field and is best accomplished through a combination of preliminary DTM evaluation before fieldwork and visual examination in the field. When elevated surface gamma activity or pollutant concentrations are found in the field, the nearest polluted neighbourhood with the same geomorphology

(sedimentary unit) must also be included in the map. Such work requires a certain level of knowledge on the shapes of fluvial sedimentary bodies; this fact is perceived as self-evident by persons from the geomorphologic field but may not be recognised by persons from the domains of chemistry or mathematics. An example of an absence of respect for fundamental geomorphological judgement in pollution mapping was discussed by Matys Grygar [64].

Pollutant distribution in all study areas (Figures 7–9) has mostly been controlled by river channel dynamics: Most of the gamma-activity hotspots coincide with recently formed point bars, i.e., lateral deposits along the inner (convex) banks of channel bends, and abandoned meanders (Figure 5B, Figure 8B–D,F) or abandoned channel loops (Figure 5A, Figure 6B,C). In the Ploučnice River floodplain, mostly coarser (sandy) sediments are deposited on point bars (sedimentary facies with a high Zr/Rb ratio in Figure 7B). Although point bar deposits are generally coarse-grained, they have always finer (silty) laminae or beds in their bodies and are usually covered by a several decimetre-thick layer of silty overbank fines, which are both rich in pollutants. The surfaces of young (active) point bars usually have a lower elevation than the floodplain floor (i.e., a flood basin or a distal floodplain level); in other words, point bars appear as curved, narrow depressions along channel bends, easily revealed by DTM (Figures 6A, 8A and 9A) and visual examination in the field. The point bar bodies are covered by plant species typical of early successional stages, i.e., species-poor pioneer plant assemblages, in Czech Republic floodplains that typically have invasive plant species, with no older shrubs and trees. The banks opposite of the point bars are usually steep, due to ongoing lateral bank erosion. The locations of point bars should certainly be included in sampling and/or surface pollution mapping in all floodplains that receive fluvially transported pollution.

Chemical pollutants in floodplains are usually associated with finer grain sizes in overbank fines, and thus overbank fines are mostly expected to be more polluted. Contrary to this expectation, the channel sediments (including sandy deposits in point bars) in some of the study areas were more polluted than the overbank fines (silty) in the distal floodplain. One of the reasons is that in-channel deposits in the studied floodplains are formed under lower discharges, when fluvially transported polluted solids are not so intensively diluted by reworking less polluted (older) sediments [4]. Although channel belt sediments are expected to only be coarse, in particular locations, both fine sediments and pollution can even be deposited directly in the channel [65]. Conversely, deposits from extreme floods can be more diluted, due to enhanced channel bank erosion [66,67]. Of course, the previous statements are valid only if the precipitation extremes and resulting floods do not cause a pollution disaster, such as a settling pond failure or a flush of temporary pollution sinks into the catchment [68]. In the latter cases, the pollution would be maximal in almost all types of fluvial deposits. Because the effects of large floods can be highly contrasting and a priori unknown, in each new floodplain pollution survey, sampling/mapping must include all geoformations: The channel belt (point bars and other possible deposits in the proximal floodplain formed under lower discharges), natural levees and distal floodplain (deposits from extreme discharges during overbank floods).

Characterisation of the pollution hotspots in the study areas can be compared with other hotspots identified in the Ploučnice River floodplains in previous studies summarised in Table 2. Three major geoformations hosting pollution hotspots have been found:

- (1) sediments in abandoned meanders and laterally shifting channels that have evolved, i.e., were filled with sediment during the U-mining climax (1971–1989); these features can be identified with GIS analysis, in particular using old maps, aerial photographs and DTM;
- (2) other sediment traps in the floodplain, such as meander scars (more ancient channels not depicted in old maps [24]); and
- (3) certain young (recently built) levees; these locations can be identified with DTM on the external banks of meander bends and by “sedimentary facies mapping”, i.e., mapping sediment grain-size in the floodplain, because they exhibit lower Al/Si and/or higher Zr/Rb ratios in the Ploučnice River floodplain.

Table 2. Overview of polluted hotspots ordered in a downstream direction. Methods used in this work are in bold.

Study Area	Hotspot Position	Methods Used	References
ES-South of Mímoň	Former depression in floodplain (meander scar?)	GIS, gamma, XRF, laboratory XRF, geostatistical analysis	[22,26]
PK-Boreček	Abandoned channel	AAS, gamma	[19]
MH-Boreček	Former depression in floodplain (old, shallow flood channel)	GIS, XRF , laboratory XRF, gamma, ERT, DEMP, OSL, geostatistics	[9,21,24,27] This work
AT1-Hradčany	Meander abandoned during U-mining	GIS, gamma , ERT, XRF , laboratory XRF, geostatistics	[9,27,31] This work
AT2-West of Hradčany	Meander-starting to cut-off	GIS, ERT, laboratory XRF	[9,31]
MS-West of Hradčany	Channel bars and natural levees	GIS, XRF, gamma, and drone maps, geostatistical analysis	[27,29] This work
TV-Veselí	Secondary river channel	GIS, gamma, XRF, laboratory XRF, geostatistical analysis	[28]
KK-by Česká Lípa	Depression in floodplain (shallow flood channel)	GIS, gamma, DEMP, XRF, laboratory XRF, geostatistical analysis	[30]

All three of these types of polluted sediment traps represent lithological and topographical heterogeneities, which can also be visualised by geophysical imaging [9,10,24]. However, the tools reported in this paper are sufficient for identification and interpretation of pollution hotspots in the studied floodplains and can thus be applicable to any polluted floodplain.

5. Conclusions

Our study demonstrated that very detailed, i.e., high-resolution analysis (field mapping) of pollutant distribution in a floodplain can be achieved with portable analytical instruments. The mapping results can then be interpreted on the basis of micro-geomorphology of the floodplain and fluvial deposition processes. GIS tools are essential for both mapping and interpretation. Gamma spectrometry can visualise pollution even if contaminants have been buried by approximately one or two-decimetres thick younger and less polluted strata, while XRF analysis has a penetration depth of less than 1 mm and can only reveal pollutants on the top surface of the analysed samples. If this consideration is taken into account, pollution mapping is a very promising tool for analysing polluted floodplains; these techniques show how unevenly pollutants are distributed in a particular landscape.

Most gamma activity in the Ploučnice floodplain was found in locations with recent channel shifts, such as point bars and abandoned meanders. Increased activities/concentrations of pollutants were also found in old (fossil) natural levees. Due to chaotic lateral channel shifts in the current channel belt visualised by GIS tools, we can predict that pollution hotspots in channel bars and levees will be reworked on a decadal timescale. Occasional meander development, also observed in the Ploučnice River, will rework the pollution in abandoned meanders in the study area on a century timescale.

Author Contributions: Conceptualization, J.E.; Data Curation, M.S., J.E. and M.H.; Formal analysis, J.E. and J.P.; Funding acquisition, T.M.G.; Investigation, M.S., J.E., M.H. and P.N.; Methodology, T.M.G., J.E. and J.P.; Project administration, J.E.; Resources, J.E.; Supervision, T.M.G.; Validation, J.P. and T.M.G.; Visualization, J.E.; Writing—original draft preparation, T.M.G., J.E. and J.P.; writing—Review and editing, J.E., T.M.G. and P.N.

Funding: This research (mapping work, fieldwork, verification of handheld XRF instruments, evaluation and graphical presentation of experimental results) was funded by the Czech Science Foundation (project No. 15-00340S).

Acknowledgments: The authors thank P. Doškář (J. E. Purkyně University in Ústí nad Labem) for fieldwork, including in situ XRF analysis, and R. Barochová, Z. Hájková and P. Vorm (Czech Academy of Sciences, Institute of Inorganic Chemistry, Řež) for laboratory processing of sediment samples and their XRF analysis. P. Vorm also contributed by performing XRF calibration for the chemical analyses of Al and Si.

Conflicts of Interest: The authors declare no conflict of interest.

References

1. Miller, J.; Barr, R.; Grow, D.; Lechler, P.; Richardson, D.; Waltman, K.; Warwick, J. Effects of the 1997 flood on the transport and storage of sediment and mercury within the Carson River valley, west-central Nevada. *J. Geol.* **1999**, *107*, 313–327. [[CrossRef](#)]
2. Ciszewski, D. Flood-related changes in heavy metal concentrations within sediments of the Biała Przemsza River. *Geomorphology* **2001**, *40*, 205–218. [[CrossRef](#)]
3. Foulds, S.A.; Brewer, P.A.; Macklin, M.G.; Haresign, W.; Betson, R.E.; Rassner, S.M.E. Flood-related contamination in catchments affected by historical metal mining: An unexpected and emerging hazard of climate change. *Sci. Total Environ.* **2014**, *476*, 165–180. [[CrossRef](#)] [[PubMed](#)]
4. Matys Grygar, T.; Elznicová, J.; Bábek, O.; Hošek, M.; Engel, Z.; Kiss, T. Obtaining isochrones from pollution signals in a fluvial sediment record: A case study in a uranium-polluted floodplain of the Ploučnice River, Czech Republic. *Appl. Geochem.* **2014**, *48*, 1–15. [[CrossRef](#)]
5. Nováková, T.; Kotková, K.; Elznicová, J.; Strnad, L.; Engel, Z.; Matys Grygar, T. Pollutant dispersal and stability in a severely polluted floodplain: A case study in the Litavka River, Czech Republic. *J. Geochem. Explor.* **2015**, *156*, 131–144. [[CrossRef](#)]
6. Wohl, E. Time and the rivers flowing: Fluvial geomorphology since 1960. *Geomorphology* **2014**, *216*, 263–282. [[CrossRef](#)]
7. Houben, P. Geomorphological facies reconstruction of Late Quaternary alluvia by the application of fluvial architecture concepts. *Geomorphology* **2007**, *86*, 94–114. [[CrossRef](#)]
8. Notebaert, B.; Houbrechts, G.; Verstraeten, G.; Broothaerts, N.; Haeckx, J.; Reynnders, M.; Govers, G.; Petit, F.; Poesen, J. Fluvial architecture of Belgian river systems in contrasting environments: Implications for reconstructing the sedimentation history. *Neth. J. Geosci.* **2011**, *90*, 31–50. [[CrossRef](#)]
9. Matys Grygar, T.; Elznicová, J.; Tůmová, Š.; Faměra, M.; Balogh, M.; Kiss, T. Floodplain architecture of an actively meandering river (the Ploučnice River, the Czech Republic) as revealed by the distribution of pollution and electrical resistivity tomography. *Geomorphology* **2016**, *254*, 41–56. [[CrossRef](#)]
10. Faměra, M.; Kotková, K.; Tůmová, Š.; Elznicová, J.; Matys Grygar, T. Pollution distribution in floodplain structure visualised by electrical resistivity imaging in the floodplain of the Litavka River, the Czech Republic. *CATENA* **2018**, *165*, 157–172. [[CrossRef](#)]
11. Matys Grygar, T.; Nováková, T.; Bábek, O.; Elznicová, J.; Vadinová, N. Robust assessment of moderate heavy metal contamination levels in floodplain sediments: A case study on the Jizera River, Czech Republic. *Sci. Total Environ.* **2013**, *452*, 233–245. [[CrossRef](#)]
12. Stacke, V.; Pánek, T.; Sedláček, J. Late Holocene evolution of the Bečva River floodplain (Outer Western Carpathians, Czech Republic). *Geomorphology* **2014**, *206*, 440–451. [[CrossRef](#)]
13. Marks, K.; Bates, P. Integration of high-resolution topographic data with floodplain flow models. *Hydrol. Process.* **2000**, *14*, 2109–2122. [[CrossRef](#)]
14. Gałuszka, A.; Migaszewski, Z.; Namieśnik, J. Moving your laboratories to the field—Advantages and limitations of the use of field portable instruments in environmental sample analysis. *Environ. Res.* **2015**, *140*, 593–603. [[CrossRef](#)] [[PubMed](#)]
15. Hürkamp, K.; Raab, T.; Voelkel, J. Two and three-dimensional quantification of lead contamination in alluvial soils of a historic mining area using field portable X-ray fluorescence (FPXRF) analysis. *Geomorphology* **2009**, *110*, 28–36. [[CrossRef](#)]
16. Weindorf, D.C.; Zhu, Y.; Chakraborty, S.; Bakr, N.; Huang, B. Use of portable X-ray fluorescence spectrometry for environmental quality assessment of peri-urban agriculture. *Environ. Monit. Assess.* **2012**, *184*, 217–227. [[CrossRef](#)] [[PubMed](#)]
17. Parsons, C.; Grabulosa, E.M.; Pili, E.; Floor, G.H.; Roman-Ross, G.; Charlet, L. Quantification of trace arsenic in soils by field-portable X-ray fluorescence spectrometry: Considerations for sample preparation and measurement conditions. *J. Hazard. Mater.* **2013**, *262*, 1213–1222. [[CrossRef](#)] [[PubMed](#)]
18. Brumbaugh, W.G.; Tillitt, D.E.; May, T.W.; Javzan, Ch.; Komov, V.T. Environmental survey in the Tuul and Orkhon River basins of north-central Mongolia, 2010: Metals and other elements in streambed sediment and floodplain soil. *Environ. Monit. Assess.* **2013**, *185*, 8991–9008. [[CrossRef](#)]

19. Kühn, J. Distribuce Uranu a Vybraných Těžkých Kovů v Sedimentech údolní Nivy Ploučnice (Distribution of Uranium and Selected Heavy Metals in Sediments of the Floodplain of the Ploučnice River). Ph.D. Thesis, Faculty of Science Charles University, Prague, Czech Republic, 1996.
20. Martin, P.G.; Payton, O.D.; Fordoulis, J.S.; Richards, D.A.; Scott, T.B. The use of unmanned aerial systems for the mapping of legacy uranium mines. *J. Environ. Radioact.* **2015**, *143*, 135–140. [[CrossRef](#)]
21. Hošek, M. Kontaminace nivy Ploučnice Těžkými Kovy ve Vztahu k Její Architektuře (Pollution of Ploučnice Floodplain by Heavy Metals in Relation to Its Architecture). Master's Thesis, Faculty of Science Charles University, Prague, Czech Republic, 2015.
22. Slabá, E.; Matys Grygar, T.; Elznicová, J. Posouzení navržených revitalizačních opatření řeky Ploučnice u Mimoň z hlediska remobilizace historické kontaminace. (Evaluation of proposed revitalization of the river Ploučnice close to Mimoň in terms of remobilization of historical contamination). In Proceedings of the Krajinné inženýrství 2015. Provoz a údržba staveb krajinného inženýrství 2015, Prague, Czech Republic, 17 September 2015; Česká společnost krajinných inženýrů: Praha, Czech Republic, 2015; pp. 105–120, ISBN 978-80-87384-07-7.
23. Elznicová, J.; Plotnárek, L. Reconstruction of historical landscape from aerial photographs for river development assessment. In Proceedings of the 14th SGEM GeoConference on Informatics, Geoinformatics and Remote Sensing, SGEM2014 Conference Proceedings, Albena, Bulgaria, 19–25 June 2014; Volume 3, pp. 269–2704, ISBN 978-619-7105-12-4. [[CrossRef](#)]
24. Hošek, M.; Matys Grygar, T.; Elznicová, J.; Faměra, M.; Popelka, J.; Matkovič, J.; Kiss, T. Geochemical mapping in polluted floodplains using in situ X-ray fluorescence analysis, geophysical imaging, and statistics: Surprising complexity of floodplain pollution hotspot. *CATENA* **2018**, *171*, 632–644. [[CrossRef](#)]
25. Elznicová, J.; Hrubešová, D. Spatiotemporal changes of the Ploučnice River for the explanation of pollution distribution in the floodplain. In Proceedings of the SGEM 2017 Conference on 17th International Multidisciplinary Scientific GeoConference SGEM 2017, Albena, Bulgaria, 29 June–5 July 2017; STEF92 Technology: Sofia, Bulgaria, 2017; Volume 17, pp. 665–672. [[CrossRef](#)]
26. Slabá, E. Posouzení Navržených Revitalizačních Opatření řeky Ploučnice u Mimoň z Hlediska Remobilizace Historické Kontaminace (Evaluation of Proposed Revitalization of the river Ploučnice Close to Mimoň in Terms of Remobilization of Historical Contamination). Master's Thesis, J.E. Purkyně University in Ústí nad Labem, Ústí nad Labem, Czech Republic, 2015.
27. Sikora, M. Zhodnocení Vývoje Radioaktivního Znečištění Toků a údolní Nivy Ploučnice (The Evaluation of Radioactive Contamination of the Ploučnice River and Floodplain). Master's Thesis, J.E. Purkyně University in Ústí nad Labem, Ústí nad Labem, Czech Republic, 2016.
28. Váchová, T. Využití Geostatických Metod Při Mapování Znečištění v Nivě řeky Ploučnice (Application of Geostatistical Methods for Mapping Pollution in the River Floodplain Ploučnice). Master's Thesis, J.E. Purkyně University in Ústí nad Labem, Ústí nad Labem, Czech Republic, 2017.
29. Elznicová, J.; Matys Grygar, T.; Sikora, M.; Popelka, J.; Hošek, M.; Novák, P. Threat of pollution hotspots reworking in river systems: Example of the Ploučnice River (Czech Republic). In Proceedings of the GIS for Safety & Security Management, GIS Ostrava 2018, Ostrava, Czech Republic, 21–23 March 2018; Ivan, I., Čaha, J., Burian, J., Eds.; VŠB Technical University of Ostrava: Ostrava, Czech Republic, 2018; pp. 159–176, ISBN 978-80-248-4235-6.
30. Klimešová, K. Mapování znečištění nivy řeky Ploučnice (Floodplain mapping of pollution of the river Ploučnice). Master's Thesis, J.E. Purkyně University in Ústí nad Labem, Ústí nad Labem, Czech Republic, 2018.
31. Típanová, A. Transport Polutantů z Těžby a Zpracování Uranu říčním Systémem Ploučnice (Transport of Pollutants from Mining and Processing of Uranium in River System Ploučnice). Master's Thesis, Department of Geology, Faculty of Science Palacký University, Olomouc, Czech Republic, 2016.
32. Vitáček, Z.; Knauerová, M.; Kühn, P. Řeka Ploučnice a Příroda v Okolí (Ploučnice River and Nature around). Mikroregion Podralsko. Available online: <http://www.podralsko.info/zelena-cyklomagistrala-ploucnice/informace-o-rece-ploucnice/> (accessed on 7 February 2018).
33. Novák, M.; Emmanuel, S.; Vile, M.A.; Erel, Y.; Véron, A.; Pačes, T.; Wieder, R.K.; Vaněček, M.; Štěpánová, M.; Břízová, E.; et al. Origin of lead in eight Central European peat bogs determined from isotope ratios, strengths, and operation times of regional pollution sources. *Environ. Sci. Technol.* **2003**, *37*, 437–445. [[CrossRef](#)] [[PubMed](#)]

34. Matys Grygar, T.; Sedláček, J.; Bábek, O.; Nováková, T.; Strnad, L.; Mihaljevič, M. Regional contamination of Moravia (south-eastern Czech Republic): Temporal shift of Pb and Zn loading in fluvial sediments. *Water Air Soil Pollut.* **2012**, *223*, 739–753. [CrossRef]
35. Majerová, L.; Matys Grygar, T.; Elznicová, J.; Strnad, L. The Differentiation between Point and Diffuse Industrial Pollution of the Floodplain of the Ploucnice River, Czech Republic. *Water Air Soil Pollut.* **2013**, *224*, 1688. [CrossRef]
36. Hrdoušek, F. Těžké kovy v sedimentech Panenského potoka a středního toku Ploučnice (Heavy metals in sediments of Panenský Creek and middle reach of Ploučnice). Master's Thesis, Faculty of Science Charles University, Prague, Czech Republic, 2005.
37. Kühn, P. Radioaktivní znečištění údolní nivy Ploučnice v bývalém VVP Ralsko (Radioactive pollution of the floodplain of the Ploučnice in former military area Ralsko). Available online: <http://www.strazpr.cz/radioaktivni-znecisten-v-severozapadni-casti-byvaleho-vvp-ralsko/d-3708> (accessed on 31 December 2018).
38. Kafka, J. *Rudné a Uranové Hornictví České Republiky (Ore and Uranium Mining in the Czech Republic)*; Anagram: Ostrava, Czech Republic, 2003; ISBN 80-86331-67-9.
39. Slezák, J. Historie těžby uranu v oblasti Stráže pod Ralskem v severočeské křídě a hydrogeologie (History of uranium production in the area of Stráž pod Ralskem (the North Bohemian Cretaceous basin) and hydrogeology). *Sbor. Geol. Věd. Hydrogeol. inž. Geol.* **2000**, *21*, 5–36.
40. Hanslík, E. *Vliv těžby Uranových Rud na vývoj Kontaminace Hydrosféry Ploučnice v Období 1966–2000 (Impact of Uranium Ore Mining on Course of Pollution of Ploučnice Hydrosphere in Period of 1966–2000)*; Výzkumný ústav vodohospodářský T.G.: Prague, Czech Republic, 2002.
41. Gnojek, I.; Dědáček, K.; Zabadal, S.; Sedlák, J. *Letecké geofyzikální mapování radioaktivních zátěží Liberecka (Aerial Geophysical Mapping of Radioactive Loads of the Liberec Area)*; Final Report; Geofond Praha (The archive of the Czech Geological Survey): Prague, Czech Republic, 2005.
42. Kolář, J. Distribuce Vybraných Těžkých Kovů v Sedimentech Horního Toku Ploučnice (Distribution of Selected Heavy Metals in Sediments of Upper Reach of Ploučnice). Master's Thesis, Faculty of Science Charles University, Prague, Czech Republic, 2004.
43. Digitální model reliéfu České republiky 5. generace (DMR 5G) (Digital Terrain Model of the Czech Republic 5th Generation). Available online: [https://geoportal.cuzk.cz/\(S\(npqw1dtiaknauys50u2ty42r\)\)/Default.aspx?lng=EN&mode=TextMeta&side=vyskopis&metadataID=CZ-CUZK-DMR5G-V&head_tab=sekce-02-gp&menu=302](https://geoportal.cuzk.cz/(S(npqw1dtiaknauys50u2ty42r))/Default.aspx?lng=EN&mode=TextMeta&side=vyskopis&metadataID=CZ-CUZK-DMR5G-V&head_tab=sekce-02-gp&menu=302) (accessed on 31 December 2018).
44. Dilts, T.E. Stream Gradient and Sinuosity Toolbox for ArcGIS 10.1. University of Nevada Reno, 2015. Available online: <http://www.arcgis.com/home/item.html?id=c8eb4ce1384e45258ccba1b33cd4e3cb> (accessed on 31 December 2018).
45. Grygar, T.; Světlík, I.; Lisá, L.; Koptíková, L.; Bajer, A.; Wray, D.S.; Ettler, V.; Mihaljevič, M.; Nováková, T.; Koubová, M.; et al. Geochemical tools for the stratigraphic correlation of floodplain deposits of the Morava River in Strážnické Pomoraví, Czech Republic from the last millennium. *CATENA* **2010**, *80*, 106–121. [CrossRef]
46. Bouchez, J.; Gaillardet, J.; France-Lanord, C.; Maurice, L.; Dutra-Maia, P. Grain size control of river suspended sediment geochemistry: Clues from Amazon River depth profiles. *Geochem. Geophys. Geosyst.* **2011**, *12*, 1525–2027. [CrossRef]
47. Bábek, O.; Matys Grygar, T.; Faměra, M.; Hron, K.; Nováková, T.; Sedláček, J. Geochemical background in polluted river sediments: How to separate the effects of sediment provenance and grain size with statistical rigour? *CATENA* **2015**, *135*, 240–253. [CrossRef]
48. Dypvik, H.; Harris, N.B. Geochemical facies analysis of fine-grained siliciclastics using Th/U, Zr/Rb and (Zr+Rb)/Sr ratios. *Chem. Geol.* **2001**, *181*, 131–146. [CrossRef]
49. Jones, A.F.; Macklin, M.G.; Brewer, P.A. A geochemical record of flooding on the upper River Severn, UK, during the last 3750 years. *Geomorphology* **2012**, *179*, 89–105. [CrossRef]
50. Vijver, M.G.; Spijker, J.; Vink, J.P.M.; Posthuma, L. Determining metal origins and availability in fluvial deposits by analysis of geochemical baselines and solid-solution partitioning measurements and modelling. *Environ. Pollut.* **2008**, *156*, 832–839. [CrossRef]
51. Jiang, J.-B.; Wang, J.; Liu, S.-Q.; Lin, C.-Y.; He, M.-C.; Li, X.-T. Background, baseline, normalization, and contamination of heavy metals in the Liao River Watershed sediments of China. *J. Asian Earth Sci.* **2013**, *73*, 87–94. [CrossRef]

52. Guo, Y.-Q.; Huang, C.-C.; Pang, J.L.; Zha, X.-C.; Li, X.P.; Zhang, Y.Z. Concentration of heavy metals in the modern flood slackwater deposits along the upper Hanjiang River valley, China. *CATENA* **2014**, *116*, 123–131. [[CrossRef](#)]
53. Wang, J.; Liu, G.-J.; Lu, L.-L.; Zhang, J.-M.; Liu, H.-Q. Geochemical normalization and assessment of heavy metals (Cu, Pb, Zn, and Ni) in sediments from the Huaihe River, Anhui, China. *CATENA* **2015**, *129*, 30–38. [[CrossRef](#)]
54. Matys Grygar, T.; Popelka, J. Revisiting geochemical methods of distinguishing natural concentrations and pollution b risk elements in fluvial sediments. *J. Geochem. Explor.* **2016**, *170*, 39–57. [[CrossRef](#)]
55. Löwemark, L.; Chen, H.-F.; Yang, T.-N.; Kylander, M.; Yu, E.-F.; Hsu, Y.-W.; Lee, T.-Q.; Song, S.-R.; Jarvis, S. Normalizing XRF-scanner data: A cautionary note on the interpretation of high-resolution records from organic-rich lakes. *J. Asian Earth Sci.* **2011**, *40*, 1250–1256. [[CrossRef](#)]
56. Oliver, M.A.; Webster, R. A tutorial guide to geostatistics: Computing and modelling variograms and kriging. *CATENA* **2014**, *113*, 56–69. [[CrossRef](#)]
57. ESRI. ArcGIS Desktop: Release 10.6. Environmental Systems Research Institute, Redlands, 2018. Available online: <http://desktop.arcgis.com/en/arcmap/latest/extensions/geostatistical-analyst/what-is-geostatistics-.htm> (accessed on 31 December 2018).
58. Wackernagel, H. *Multivariate Geostatistics: An Introduction with Applications*; Springer: Berlin, Germany, 2003; p. 25. ISBN 978-3-662-05294-5.
59. Li, J.; Heap, A.D. *A Review of Spatial Interpolation Methods for Environmental Scientists*; Record 2008/23; Geoscience Australia: Canberra, Australia, 2008; pp. 154–196. ISBN 978-1-921498-28-2.
60. Burrough, P.A.; McDonnell, R.; McDonnell, R.A.; Lloyd, C.H.D. *Principles of Geographical Information Systems*; Oxford University Press: Oxford, UK, 2015; p. 174. ISBN 978-0-19-874284-5.
61. Zuo, X.; Zhao, H.; Zhao, X.; Zhang, T.; Guo, Y.; Wang, S.; Drake, S. Spatial pattern and heterogeneity of soil properties in sand dunes under grazing and restoration in Horqin Sandy Land, Northern China. *Soil Tillage Res.* **2008**, *99*, 202–212. [[CrossRef](#)]
62. Argyraki, A.; Ramsey, M.H.; Potts, P.J. Evaluation of Portable X-ray Fluorescence Instrumentation for in situ Measurements of Lead on Contaminated Land. *Analyst* **1997**, *122*, 743–749. [[CrossRef](#)]
63. Weindorf, D.C.; Bakr, N.; Zhu, Y.; Mcwhirt, A.; Ping, C.L.; Michaelson, G.; Nelson, C.; Shook, K.; Nuss, S. Influence of Ice on Soil Elemental Characterization via Portable X-Ray Fluorescence Spectrometry. *Pedosphere* **2014**, *24*, 1–12. [[CrossRef](#)]
64. Matys Grygar, T. Letter to Editor re Pavlović et al. (2015). *Sci. Total Environ.* **2016**, *547*, 482–483. [[CrossRef](#)]
65. Ciszewski, D. Channel processes as a factor controlling accumulation of heavy metals in river bottom sediments: Consequences for pollution monitoring (Upper Silesia, Poland). *Environ. Geol.* **1998**, *36*, 45–54. [[CrossRef](#)]
66. Navrátil, T.; Rohovec, J.; Žák, K. Floodplain sediments of the 2002 catastrophic flood at the Vltava (Moldau) River and its tributaries: Mineralogy, chemical composition, and post-sedimentary evolution. *Environ. Geol.* **2008**, *56*, 399–412. [[CrossRef](#)]
67. Bábek, O.; Faměra, M.; Hilscherová, K.; Kalvoda, J.; Dobrovolný, P.; Sedláček, J. Geochemical traces of flood layers in the fluvial sedimentary archive; implications for contamination history analyses. *CATENA* **2011**, *87*, 281–290. [[CrossRef](#)]
68. Dhivert, E.; Grosbois, C.; Rodrigues, S.; Desmet, M. Influence of fluvial environments on sediment archiving processes and temporal pollutant dynamics (Upper Loire River, France). *Sci. Total Environ.* **2015**, *505*, 121–136. [[CrossRef](#)] [[PubMed](#)]

